

Disease dynamics in metapopulations

Veronika Siska

Erasmus Mundus (M1) project report (20ECTS)
Department of Physics
University of Gothenburg
2013

Faculty of Science



UNIVERSITY OF GOTHENBURG

Abstract

Structured populations are of particular interest when discussing disease dynamics. A common approach is to consider metapopulations: a group of coupled, well-mixed patches (also called (sub)populations or households). Two, frequently used ways to realize coupling are to introduce between-patch contact rates and to allow migration. Although these two ways describe different real-life situations, they result in similar dynamics under certain conditions.

My project consists of two parts. In the first part, I focused on two different metapopulation models, both consisting of equally-sized, well-mixed, coupled patches. The first model consisted of subpopulations with standard SIR (susceptible-infected-recovered) dynamics, coupled by contact. In the second model, a latent period was introduced and patches were coupled by migration, but infectives were not allowed to migrate. For both of the models, stochastic individual-based models and the corresponding deterministic dynamics in the limit of an infinite number of (not necessarily large) patches were constructed and compared. The results imply equivalence for weak coupling.

In the second part, I focus on the Tasmanian Devil Facial Tumour Disease (DFTD), an infectious cancer that threatens the species of tasmanian devils, the largest marsupial carnivore with extinction. I developed a stochastic, spatial, age-structured SEI model consisting of well-mixed patches with nearest neighbour interaction: migration and contact. I used parameter estimations from the literature, where available, and fit the rest of the parameters to published data. Results showed that migration was required for a healthy population to survive despite the strong demographic fluctuations and contact was needed to match the speed of the spatial spread. In the future, I will apply my model to make predictions and investigate possible control measures.

Acknowledgements

I would like to express my gratitude to my supervisor Bernhard Mehlig for introducing me to the topic as well for the support on the way. Without his guidance and persistent help this project would not have been possible. Furthermore, I would like to thank Anders Eriksson for his co-supervision on the second part of my project and providing insightful comments and suggestions besides the initial idea on both parts. I am also grateful for Andrea Manica for his warm encouragement and co-supervision during the second part of my project.

I would like to thank all members of the Department of Physics with whom I interacted during the course of my project for welcoming me. I would particularly like to thank Jonas Einarsson for his help on practical details and my roommates from the master student's room for creating a cheerful atmosphere. I would also like to express my gratitude to Erasmus Mundus consortium for their financial support.

Veronika Siska, Gothenburg 2013 July 2

Contents

1	Introduction	1
1.1	Local dynamics	1
1.2	Metapopulations	2
2	Homogeneous models	4
2.1	Definition of the models	4
2.1.1	Contact model	4
2.1.2	Migration model with latency	5
2.2	Stochastic simulations	6
2.3	Deterministic equations	6
2.3.1	Contact model	7
2.3.2	Migration model	8
2.4	Comparison between stochastic and deterministic dynamics	10
2.5	Applications	10
2.5.1	Calculating R^* from the deterministic dynamics	10
2.5.2	Future applications	13
3	Application - DFTD	16
3.1	Introduction	16
3.1.1	The Tasmanian devil	16
3.1.2	Tasmanian Devil Facial Tumour Disease (DFTD)	17
3.2	Previous models	17
3.3	My spatial model	18
3.4	Fitting the model	20
3.4.1	Parameters to fit	20
3.4.2	Response variables	20
3.4.3	Results	22
3.5	Future work	23
	Bibliography	29

A	Local model	30
A.1	SEIR model and its deterministic approximation	30
A.2	Stochastic simulations	31
A.3	Master equation	33
A.4	Limit of infinite population	34
B	Standard metapopulation	36
B.1	Introduction	36
B.2	Deterministic dynamics	36
B.3	Comparison of distributions	37

1

Introduction

The influence of spatial structure in population dynamics, including disease dynamics have been studied intensively in the recent years. One way to incorporate structure is to consider metapopulations, consisting of well-mixed, coupled patches, also called populations or households. The reproductive ratio R_0 is an important quantity in all models, determining the behaviour of the system, but it is less straightforward to define in structured populations.

1.1 Local dynamics

In metapopulation models, the patches are usually thought to be homogeneously mixed, containing individuals in different states of the disease. There are several choices for the underlying local dynamics and they can be classified according to the considered phases of the disease (compartments) and the reaction between them.

The commonly considered types of individuals are susceptible (S), exposed (E), infected (I) and recovered (R). The models are generally named after these compartments, for example the standard SIR model uses only susceptible, infected and recovered individuals, with a constant population size. Susceptibles can be infected by infectives and can first turn exposed, carrying the disease but not infecting yet. Infected individuals can recover. Exposed individuals can be disregarded, corresponding to a lack of latent period and infected individuals can be removed from the dynamics instead of recovering.

The behaviour of the system is fundamentally different if we allow the recruitment of susceptibles. Recruitment can occur through natural birth- and death processes (e.g. SIR_{BD} : SIR dynamics with birth and death [1][2][3], $SEIR_{BD}$: [4]), individuals returning to the susceptible pool after the last phase of the disease (e.g. $SIRS$ [1]) or the combination of the two (e.g. SIS_{BD} [5]). In models with recruitment, an endemic stable steady state can exist in an infinite population for $R_0 > 1$. Without recruitment, however, the only steady-state is disease-free, but the number of infectives initially grow

for $R_0 > 1$. The time to extinction is infinity for an infinite population in both cases, but becomes finite for a finite population.[6]

During my general investigations, I will use the standard SIR and SEIR models for the local dynamics (no recruitment, with/without latency). A more detailed description and analysis is included in appendix A. In my application for DFTD, however, the time-scales of the disease and the demography of the devil are not separated and thus natural birth- and death processes has to be taken into account. Moreover, the disease has a long latent period and is lethal, so I used the $SEIBD$ model.

Density-dependent versus frequency-dependent infection rate The infection rate λ in all of the above described models can be defined to be either "density-dependent": $\lambda = \eta SI$ or "frequency-dependent": $\lambda = \eta SI/N$, where η is a constant, S is the number of susceptibles, I is the number of infectives and N is the population size. Note, that if the patch sizes are all equal and constant, the difference is only a constant factor. It is the case for my general investigations (precisely for the contact model and approximately for the migration model), but not for my application.

The "density-dependent" case corresponds to a constant individual-to-individual contact rate, leading to the total number of contacts an individual makes to be proportional to the population size. As a result, the contact rate and the basic reproductive number R_0 is also proportional to the population size, leading to the extinction of the disease under a critical size, determined by $R_0 = 1$ [6].

The "frequency-dependent" case, on the other hand, corresponds to all individuals creating a fixed number of contacts, independent of the population size. As a result, R_0 is also independent of the population size, and - provided that $R_0 > 1$ initially - the disease does not die out in a decreasing population. Consequentially, such a disease (like, apparently, the devil facial tumor disease in tasmanian devils) can lead to the extinction of its host [7].

1.2 Metapopulations

Metapopulations are formed by well-mixed, coupled patches. In a standard metapopulation model, the local dynamics consist only of natural birth and death while patches are connected by migration (detailed description and analysis in appendix B). In order to investigate the spreading of infections, I used compartmental epidemiological models for the local dynamics, as described in section 1.1.

Coupling There are two main methods to enable coupling in a metapopulation with disease dynamics. The first is to allow individuals on different patches to contact each other (e.g. [8][9] for the SIR and [10][11] for the SEIRS model, all with homogeneous coupling). The second is to include migration. For example, in [2], no spacial structure while [12] uses a lattice and [13] a complex spatial structure. The main effect, between-patch spread, is the same for both, but migration also has a secondary effect on the local dynamics. The equivalence of contact and migration for two infinite patches was

investigated by looking at the eigenvalues of the corresponding deterministic differential equation system [14]. Other ways of connection are possible, such as adding special individuals, belonging to multiple patches [15].

I will consider both contact and migration, in the first part of my report by comparing them in a homogeneous model. In the second part, describing the application for Devil Facial Tumour Disease, I will use a model realizing contact and migration simultaneously.

Structure In the simplest case, without spatial structure, any patch interacts with any other equally likely [8][9][2]. However, the need to consider spatial structure arises naturally once we would like to apply a metapopulation model: homogeneous contacts among patches is the easiest to analyse, but often not very realistic. The simplest way is to consider a two-dimensional lattice, with a patch on each cell and allow homogeneous nearest-neighbour interaction only [16][12][1]. An even more realistic way is to construct a contact network between the patches [13], but it raises the number of parameters in the model considerably.

I will investigate homogeneous, all-to-all interactions in the general case and a lattice-like structure with unequal patch sizes but homogeneous nearest-neighbour interactions for my application on the Tasmanian Devil Facial Tumour Disease.

Reproductive number The local reproductive number is defined as the expected number of infections caused by a typical infectious individual in a completely susceptible population. For a metapopulation, a "typical infectious individual" is less straightforward to define; different reproductive numbers can be used, all with the same threshold behaviour: the disease can only spread if it is larger than unity [17]. The most common version is the group/household reproductive number: the number of patches contacted by a patch containing a single initial infective during its lifetime, while disregarding the effect of other patches [8][9][18][19][17][11][15].

2

Homogeneous models

I first conducted an analysis on metapopulations with homogeneous mixing. My goal was to investigate how the two most common ways of coupling, contact and migration, effect the dynamics, together with latency. In order to achieve this, I derived the deterministic counterpart of two stochastic models, in the limit of an infinite number of patches. I compared the models through examining the group reproductive number, a quantity fundamentally determining the behaviour of the system.

2.1 Definition of the models

Both of the investigated models consist of homogeneously coupled, well-mixed patches. The local dynamics are according to a compartmental model without recruitment, assuming a recovered class and thus a constant population size. The first model consists of simple SIR patches coupled by contact, identical to that described in [8]. I will refer to this model as the "contact model". The second, that I will refer to as the "migration model with latency", consists of SEIR patches, coupled by the migration of all individuals except for infectives.

2.1.1 Contact model

In the contact model, the local dynamics are according to the standard, stochastic SIR dynamics. Moreover, individuals make global contacts at the points of a Poisson process with rate λ_G , corresponding to an individual-to-individual rate of λ_L/N_{pop} , where $N_{pop} = NK$ is the (constant) population size, N the number of patches and K the number of individuals per patch (carrying capacity). Consequently, the possible events are local infection, global infection and recovery, with rates and effects as shown on table 2.1.

This model is the simplest case of the so-called "epidemic models with two levels of mixing". They are studied deeply in [8], including a simple formula for the group

Process	Rate	Effects
Local infection	$\lambda_L S_i I_i$	$I_i \rightarrow I_i + 1, S_i \rightarrow S_i - 1$
Global infection	$\frac{\lambda_G}{N_{pop}} S_i \sum_j I_j$	$I_i \rightarrow I_i + 1, S_i \rightarrow S_i - 1$
Recovery	I_i / τ_I	$I_i \rightarrow I_i - 1, R_i \rightarrow R_i + 1$

Table 2.1: Rates and effects of possible events on patch i consisting of S_i susceptibles, I_i infected and R_i recovered individuals for the contact model.

Process	Rate	Effects
Infection	$\eta S_i I_i$	$E_i \rightarrow E_i + 1, S_i \rightarrow S_i - 1$
Outbreak	E_i / τ_U	$I_i \rightarrow I_i + 1, E_i \rightarrow E_i - 1$
Recovery	I_i / τ_I	$I_i \rightarrow I_i - 1, R_i \rightarrow R_i + 1$
Emigration (class X)	$m X_i$	$X_i \rightarrow X_i - 1$
Immigration (class X)	$\frac{1}{N} \sum_j m X_j$	$X_i \rightarrow X_i + 1$

Table 2.2: Rates and effects of possible events on patch i consisting of S_i susceptibles, E_i exposed, I_i infected and R_i recovered individuals for the migration model with latency.

reproductive number R^* . Different reproductive numbers, all with the same threshold behaviour are described in [17], while the real-time growth rate r_0 is discussed in [19].

The group reproductive number in the above described, simple model can be calculated from the following formula

$$R^* = \lambda_G \mu \tau_I, \quad (2.1)$$

where μ is the expected size of the local epidemic [8].

2.1.2 Migration model with latency

In the migration model with latency, the local dynamics are according to the standard SEIR dynamics. Moreover, individuals except for infectives are allowed to migrate. Every individual emigrates with a constant rate m to a randomly chosen destination, instantaneously. As a result, the possible events are infection, outbreak and migration, with the rates and effects shown on table 2.2.

It is less straightforward to determine a simple formula for the group reproductive number in the migration model than in the contact model, due to the secondary effects of migration on the local dynamics. Since emigrated individuals, once turning infected, can not migrate any more, global infectious are caused solely by exposed migrants. Consequently, if the size of the local epidemic is not affected by migration, an approximation for the group reproductive number would be the following:

$$R^* = \mu P_d, \quad (2.2)$$

where μ is the expected size of the local epidemic and P_d is the probability that an exposed individual emigrates before falling ill. In our model, using the Poisson approximation for all processes, the dispersal probability P_d is

$$P_d = \frac{m}{m + 1/\tau_E} \quad (2.3)$$

The above formula was inspired by an apparent scaling relation between the migration rate m and the average latent period $1/\tau_E$: both the average size of an epidemic and the probability of a large outbreak seems to depend on these two parameters only through P_d (figure 2.1).

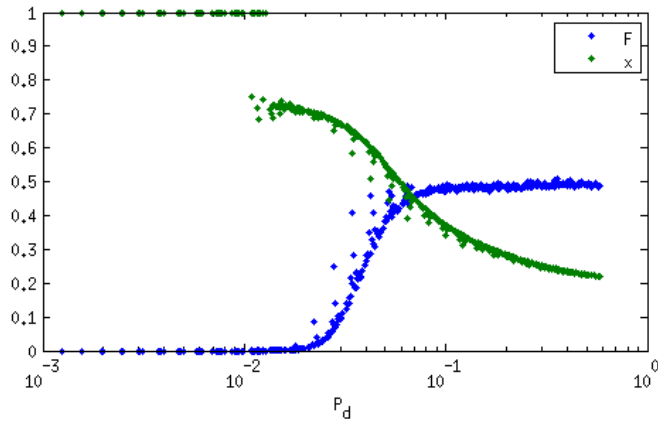


Figure 2.1: Fraction of susceptibles x unaffected by the epidemic conditional on a large outbreak ($x < 0.25$) and the fraction of cases resulting in a large outbreak F for $\eta = 0.005$, $\tau_I = 4$, $K = 100$, $N = 200$ and averaging for 2000 simulations. m and τ_E were varied independently of each other in the intervals $m \in [0.001, 0.1]$ and $\tau_E \in [1, 20]$.

2.2 Stochastic simulations

The starting point in investigating disease spreading in a metapopulation was a stochastic, individual-based model. All processes are assumed to be Poisson processes with the appropriate rates. I use continuous-time models: in each step, the sum of all rates are computed, an event on a patch is chosen with probabilities proportional to their rates and the elapsed time between two events is drawn from an exponential distribution with its parameter equal to the sum of all rates, as shown on tables 2.1 and 2.2.

2.3 Deterministic equations

In order to derive the deterministic dynamics, I considered the limit of an infinite number of patches in each model. The main variable was first the number of patches in a given

Process	Rate in state (i,j)	Terms with positive contribution to $df_{i,j}/dt$
Local infection	$\lambda_L i j$	$f_{i-1,j+1} - 1/N \rightarrow f_{i-1,j+1},$
Global infection	$\frac{\lambda_G}{K} i \sum_{i,j} j f_{i,j}$	$f_{i,j} + 1/N \rightarrow f_{i,j}$
Recovery	j/τ_I	$f_{i,j-1} - 1/N \rightarrow f_{i,j-1}, f_{i,j} + 1/N \rightarrow f_{i,j}$

Table 2.3: Contributions to the master equation in the contact model

local state (\mathbf{n}), described by the number of individuals in each compartment. The common approach then is to consider the master equation for the change in time of $\rho(\mathbf{n})$, the probability of observing the (global) state described by \mathbf{n} .

In order to acquire smooth functions for large number of patches, it is convenient to use the fraction of patches $\mathbf{f} = \mathbf{n}/N$ as a variable. Next, we can consider the limit of an infinite number of patches $N \rightarrow \infty$ by considering only the zeroth order terms in the $1/N$ expansion of the master equation. It usually yields a transfer equation with some velocity \mathbf{v} , which will thus be the velocity of \mathbf{f} in the deterministic model.

Moreover, to nicely formulate the master equation, a shift operator acting on a function of a function of, for example, s, e, i, r can be defined and - for continuous functions - expressed in terms of derivatives as following:

$$E_{s,e,i,r}^{\pm} g(f_{0,0,0,0}, \dots, f_{s,e,i,r}, \dots) = g(\dots, f_{s,e,i,r} \pm 1/N, \dots) = \sum_{k=0}^{\infty} \frac{(\pm 1/N)^k}{k!} \frac{\partial^k g}{\partial f_{s,e,i,r}^k} = e^{\pm \frac{1}{N} \frac{d}{df_{s,e,i,r}}} g(s, e, i) \quad (2.4)$$

Shift operators for a different number of variables are defined analogously.

2.3.1 Contact model

As the size of each patch is constant K and there are only three types of individuals, two indices are enough to describe a state in the contact model. I will denote the fraction of patches containing i susceptibles, j infectives and $K - i - j$ recovered individuals by $f_{i,j}$ and the probability that the system is in state $f_{i,j}$ by $\rho(f_{i,j})$. The processes contributing to the time derivative of $f_{i,j}$ are shown in table 2.3.

After collecting all terms and using the shift operator as defined in (2.4), the following master equation can be obtained:

$$\begin{aligned} \frac{d\rho}{dt} = & \sum_{i,j} E_{i-1,j+1}^- E_{i,j}^+ \lambda_L i j N f_{i,j} \rho + \\ & \sum_{i,j} E_{i-1,j+1}^- E_{i,j}^+ \frac{\lambda_G}{K} i < j > N f_{i,j} \rho + \sum_{i,j} E_{i,j-1}^- E_{i,j}^+ j / \tau_I N f_{i,j} \rho \end{aligned} \quad (2.5)$$

where $< j > = \sum_{k,l} l f_{k,l}$ is the average number of infectives on a patch.

After expanding the above equation in $1/N$ to the first order, a transfer equation for ρ can be obtained, corresponding to the deterministic equation $df_{i,j}/dt = v_{i,j}$ where

$$v_{i,j} = (i+1)(\lambda_L(j-1) + \lambda_G \langle j \rangle / K) f_{i+1,j-1} + \frac{1}{\tau_I}(j+1)f_{i,j+1} - (\lambda_L ij + \lambda_G i \langle j \rangle / K + j/\tau_I) f_{i,j} \quad (2.6)$$

2.3.2 Migration model

I first characterise a state by the number of patches with a certain number of susceptible, exposed, infected and recovered individuals, denoted by $n_{s,e,i,r}$. The probability of such a state is $\rho(n_{s,e,i,r})$ (note, that all indices (s,e,i,r) cover the range $[0,\infty)$). Changes in ρ originate from the disease dynamics: infection, outbreak, recovery and from immigration and emigration for the three types of mobile individuals, with contributions as shown in table 2.4.

Thus the following master equation can be obtained:

$$\begin{aligned} \frac{d\rho}{dt} = & \sum_{i,j,k,l=0}^{\infty} (E_{i,j,k,l}^+ E_{i-1,j+1,k,l}^- - 1) \alpha_{i,j,k,l} N f_{i,j,k,l} + \\ & \sum_{s,e,i,r=0}^{\infty} (E_{i,j,k,l}^+ E_{i,j-1,k+1,l}^- - 1) \beta_{i,j,k,l} N f_{i,j,k,l} + \\ & \sum_{i,j,k,l=0}^{\infty} (E_{i,j,k,l}^+ E_{i,j,k-1,l+1}^- - 1) \gamma_{s,e,i,r} N f_{i,j,k,l} + \\ & \sum_{i,j,k,l} \sum_{p,q,r,s} N (E_{i-1,j,k,l}^- E_{i,j,k,l}^+ E_{p,q,r,s}^+ E_{p+1,q,r,s}^- - 1) m_i f_{i,j,k,l} \\ & (f_{p,q,r,s} - \delta_{ip} \delta_{jq} \delta_{kr} \delta_{ls} / N + \delta_{i-1,p} \delta_{jq} \delta_{kr} \delta_{ls} / N) + \\ & \sum_{s,e,i,r} \sum_{p,q,r,s} N (E_{i,j-1,k,l}^- E_{i,j,k,l}^+ E_{p,q,r,s}^+ E_{p,q+1,r,s}^- - 1) m_i f_{i,j,k,l} \\ & (f_{p,q,r,s} - \delta_{ip} \delta_{jq} \delta_{kr} \delta_{ls} / N + \delta_{ip} \delta_{j-1,q} \delta_{kr} \delta_{ls} / N) + \\ & \sum_{i,j,k,l} \sum_{p,q,r,s} N (E_{i,j,k,l-1}^- E_{i,j,k,l}^+ E_{p,q,r,s}^+ E_{p,q,r,s+1}^- - 1) m_i f_{i,j,k,l} \\ & (f_{p,q,r,s} - \delta_{ip} \delta_{jq} \delta_{kr} \delta_{ls} / N + \delta_{ip} \delta_{jq} \delta_{kr} \delta_{l-1,s} / N), \end{aligned} \quad (2.7)$$

where I is the immigration rate which can be expressed, for example for exposed individuals, as following:

$$I_E = \frac{1}{N} \sum_{s,e,i,r=0}^{\infty} m_e n_{s,e,i,r} \quad (2.8)$$

The above equation can be expanded in $1/N$, using (2.4). In the limit of infinitely many patches, only the first non-vanishing term remains, resulting in a transfer equation of the form

$$\frac{d\rho}{dt} = - \sum_{i,j,k,l=0}^{\infty} \frac{\partial}{\partial f_{ijkl}} (v_{ijkl} \rho) \quad (2.9)$$

Process	Sign	Effect	Contribution
infection (on ijkl)	+	$n_{i-1,j+1,k,l} - 1 \rightarrow n_{i-1,j+1,k,l}$ $n_{ijkl} + 1 \rightarrow n_{ijkl}$	$\alpha_{ijkl}(n_{ijkl} + 1) \times$ $\rho(\dots, n_{i-1,j+1,k,l} - 1, \dots, n_{ijkl} + 1, \dots)$
	-	$n_{ijkl} \rightarrow n_{ijkl} - 1$ $n_{i-1,j+1,k,l} \rightarrow n_{i-1,j+1,k,l} + 1$	$\alpha_{ijkl} n_{ijkl} \rho$
outbreak (on ijkl)	+	$n_{i,j-1,k+1,l} - 1 \rightarrow n_{i,j-1,k+1,l}$ $n_{ijkl} + 1 \rightarrow n_{ijkl}$	$\beta_{ijkl}(n_{ijkl} + 1) \times$ $\rho(\dots, n_{i,j-1,k+1,l} - 1, \dots, n_{ijkl} + 1, \dots)$
	-	$n_{ijkl} \rightarrow n_{ijkl} - 1$ $n_{i,j-1,k+1,l} \rightarrow n_{i,j-1,k+1,l} + 1$	$\beta_{ijkl} n_{ijkl} \rho$
recovery (on ijkl)	+	$n_{i,j,k-1,l+1} - 1 \rightarrow n_{i,j,k-1,l+1}$ $n_{ijkl} + 1 \rightarrow n_{ijkl}$	$\gamma_{ijkl}(n_{ijkl} + 1) \times$ $\rho(\dots, n_{i,j,k-1,l+1} - 1, \dots, n_{ijkl} + 1, \dots)$
	-	$n_{ijkl} \rightarrow n_{ijkl} - 1$ $n_{i,j,k-1,l+1} \rightarrow n_{i,j,k-1,l+1} + 1$	$\gamma_{ijkl} n_{ijkl} \rho$
migration (S) (on ijkl)	+	$n_{i-1,j,k,l} - 1 \rightarrow n_{i-1,j,k,l}$ $n_{i,j,k,l} + 1 \rightarrow n_{i,j,k,l}$ $n_{p+1,q,r,s} - 1 \rightarrow n_{p+1,q,r,s}$ $n_{p,q,r,s} + 1 \rightarrow n_{p,q,r,s}$	$\frac{1}{N} \sum_{p,q,r,s=0}^{\infty} m_i (n_{ijkl} + 1) \times$ $(n_{pqrs} + 1 - \delta_{ip} \delta_{jq} \delta_{kr} \delta_{ls} + \delta_{i-1,p} \delta_{jq} \delta_{kr} \delta_{ls})$
	-	$n_{s,e,i,r} \rightarrow n_{s,e,i,r} - 1$ $n_{s-1,e,i,r} \rightarrow n_{s-1,e,i,r} + 1$	$m_s n_{seir} \rho$
migration (E) (on ijkl)	+	$n_{i,j-1,k,l} - 1 \rightarrow n_{i,j-1,k,l}$ $n_{i,j,k,l} + 1 \rightarrow n_{i,j,k,l}$ $n_{p,q+1,r,s} - 1 \rightarrow n_{p,q+1,r,s}$ $n_{p,q,r,s} + 1 \rightarrow n_{p,q,r,s}$	$\frac{1}{N} \sum_{p,q,r,s=0}^{\infty} m_j (n_{ijkl} + 1) \times$ $(n_{pqrs} + 1 - \delta_{ip} \delta_{jq} \delta_{kr} \delta_{ls} + \delta_{ip} \delta_{j-1,q} \delta_{kr} \delta_{ls})$
	-	$n_{s,e,i,r} \rightarrow n_{s,e,i,r} - 1$ $n_{s,e-1,i,r} \rightarrow n_{s,e-1,i,r} + 1$	$m_e n_{seir} \rho$
migration (R) (on ijkl)	+	$n_{i,j,k,l-1} - 1 \rightarrow n_{i,j,k,l-1}$ $n_{i,j,k,l} + 1 \rightarrow n_{i,j,k,l}$ $n_{p,q,r,s+1} - 1 \rightarrow n_{p,q,r,s+1}$ $n_{p,q,r,s} + 1 \rightarrow n_{p,q,r,s}$	$\frac{1}{N} \sum_{p,q,r,s=0}^{\infty} m_l (n_{ijkl} + 1) \times$ $(n_{pqrs} + 1 - \delta_{ip} \delta_{jq} \delta_{kr} \delta_{ls} + \delta_{ip} \delta_{jq} \delta_{kr} \delta_{l-1,s})$
	-	$n_{s,e,i,r} \rightarrow n_{s,e,i,r} - 1$ $n_{s,e,i,r-1} \rightarrow n_{s,e,i,r-1} + 1$	$m_r n_{seir} \rho$

Table 2.4: Contributions to the master equation in the migration model with latency

where

$$v_{ijkl} = \alpha_{i+1,j-1,k,l}f_{i+1,j-1,k,l} + \beta_{i,j+1,k-1,l}f_{i,j+1,k-1,l} + \gamma_{i,j,k+1,l-1}f_{i,j,k+1,l-1} - \quad (2.10)$$

$$(\alpha_{ijkl} + \beta_{ijkl} + \gamma_{ijkl} + I_S + I_E + I_R + m_i + m_j + m_l)f_{ijkl} +$$

$$I_S f_{i-1,j,k,l} + I_E f_{i,j-1,k,l} + I_R f_{i,j,k,l-1} + m_{i+1}f_{i+1,j,k,l} + m_{j+1}f_{i,j+1,k,l} + m_{l+1}f_{i,j,k,l+1}$$

This corresponds to the deterministic dynamics

$$\frac{df_{ijkl}}{dt} = v_{ijkl} \quad (2.11)$$

2.4 Comparison between stochastic and deterministic dynamics

First, I compared the deterministic dynamics to the stochastic model, using an individual-based simulation and numerically integrating the deterministic dynamics. I recorded the distribution of susceptibles $f_S = \sum_{jkl} f_{ijkl}$ after the epidemic ended in both cases. The results agreed, with better agreement for a higher number of patches in the stochastic simulations, as expected. Some results are shown on figures 2.2 and 2.3).

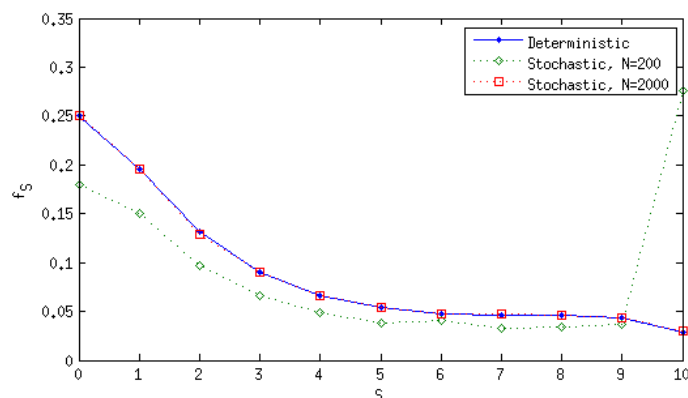


Figure 2.2: Distribution of the number of susceptibles on a patch after the epidemic has passed in the contact model for one of the parameter sets examined ($K = 10$, $\lambda_L = 0.2$, $\lambda_G = 0.5$, $\tau_I = 1$). Averaging for 50 simulations in the stochastic case.

2.5 Applications

2.5.1 Calculating R^* from the deterministic dynamics

The group reproductive number, R^* is defined as the number of patches infected by a patch with a single initial infective while all other patches are susceptible and thus can be determined from the deterministic dynamics.

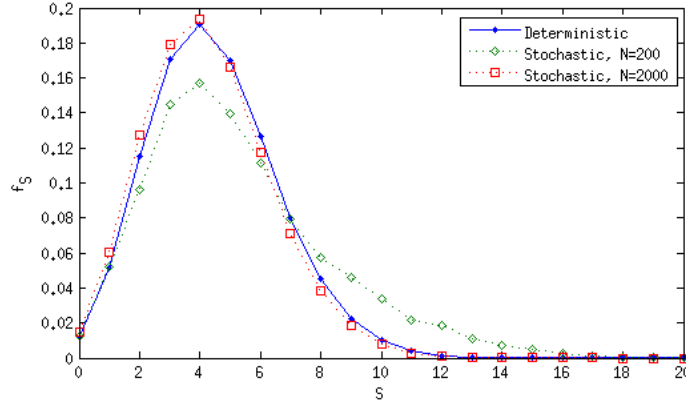


Figure 2.3: Distribution of the number of susceptibles on a patch after the epidemic has passed in the migration model with latency for one of the parameter sets examined ($K = 10$, $\eta = 0.2$, $\tau_E = 2$, $\tau_I = 2$, $m = 0.1$). Averaging for 50 simulations in the stochastic case.

Contact model

In the contact model, assuming that all global contacts target a susceptible patch (as it is the case in our approximation of an infinite number of susceptible patches), it is the number of global contacts made by a single patch over its lifetime. In terms of the dynamics, it corresponds to integrating the global contact rate over time, while disabling global contacts (which does not effect local dynamics in the limit of $N \rightarrow \infty$):

$$R_0 = \int_{t=0}^{\infty} \lambda_G I = \int_{t=0}^{\infty} \lambda_G \sum_{i,j=0}^{\infty} f_{i,j} j \quad (2.12)$$

The initial condition was set to $f_{i,j} = \delta_{K-1,1}$ where δ is the Kronecker delta, corresponding to a single initial infective on each patch. Since the local epidemic lasts forever in a deterministic model, I ran the simulation until the number of infectives or susceptibles per patch dropped below a pre-defined threshold (10^{-16}).

I performed a quick comparison with the result from [8]: $R^* = \mu \lambda_G \tau_I$, determining μ from a stochastic, individual-based, local simulation. The two group reproductive numbers agreed, as shown on figure 2.4.

Migration model with latency

In the migration model with latency, patches can only be infected globally by an exposed migrant. Consequentially, the group reproductive ratio R^* can be determined by counting exposed migrants from a patch with a single initial infective during its lifetime

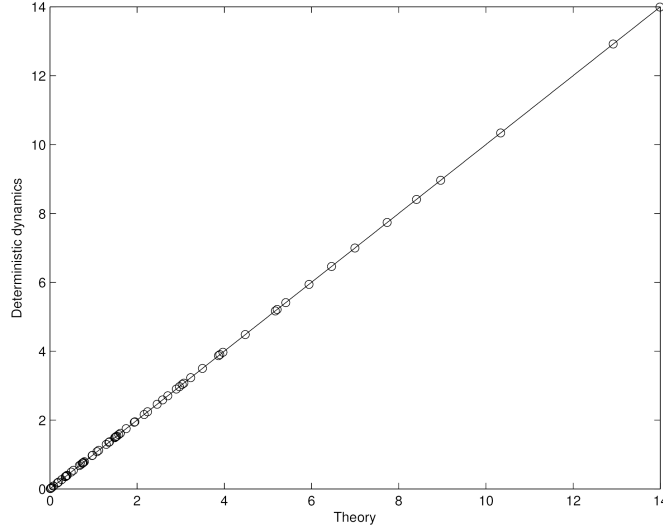


Figure 2.4: Group reproductive number R^* obtained from integrating the modified deterministic dynamics and using the result from [8]. All parameters have been varied, solid line marks the identity function.

in absence of immigration, corresponding to:

$$R_0 = \int_{t=0}^{\infty} I_E \quad (2.13)$$

where $I_E = m \sum_{ijkl} j f_{ijkl}$ is the immigration rate where f_{ijkl} is obtained from the modified dynamics, without immigration:

$$\begin{aligned} v_{ijkl} = & \alpha_{i+1,j-1,k,l} f_{i+1,j-1,k,l} + \beta_{i,j+1,k-1,l} f_{i,j+1,k-1,l} + \gamma_{i,j,k+1,l-1} f_{i,j,k+1,l-1} - (2.14) \\ & (\alpha_{ijkl} + \beta_{ijkl} + \gamma_{ijkl} + I_S + I_E + I_R + m_i + m_j + m_l) f_{ijkl} + \\ & m_{i+1} f_{i+1,j,k,l} m_{j+1} f_{i,j+1,k,l} + m_{l+1} f_{i,j,k,l+1} \end{aligned}$$

Just like in the previous case, this approximation requires that all exposed migrants arrive at a different, completely susceptible patch, which is the case as long as a patch is among an infinite number of completely susceptible patches. The initial condition was analogous with the previous case: $f_{se,i,r} = \delta_{K-1,1,0,0}$.

Comparison

By comparing equations 2.1 and 2.2, our expectation is that the reproductive ratio will be the same for $\lambda_G \tau_I = P_d = \frac{m}{m+1/\tau_E}$. In order to investigate, under what circumstances this assumption is true, I determined R_0 from the deterministic dynamics in both cases.

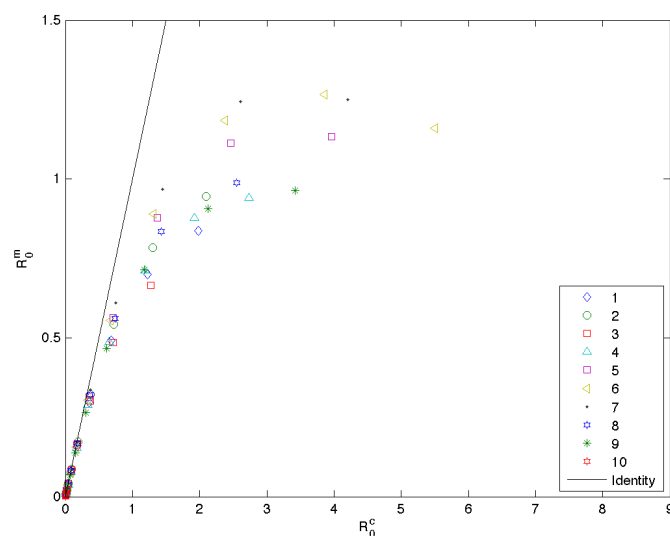


Figure 2.5: Basic reproductive numbers for Ball’s model with global contacts and our model with migration for different parameters.

My results are shown on figures 2.5 and 2.6 and the parameters used are explained in table 2.5.

What we can see on these figures is that the two models agree for small dispersal probabilities. The relative difference starts linearly, indicating that if we would expand the expressions for R_0 for the two models, they would first differ in the second order term. Agreement for $P_d = 0$ is trivial, since the only difference in the local models is latency, but that does not influence R_0 in a model without recruitment. An identical first order term, on the other hand, is not trivial, it implies that the approximation works for weak coupling. The difference in the second order term probably corresponds to the secondary effect of migration on the local dynamics.

A clearly visible property of R_0 for the model with migration is that it saturates, caused by the fact that the dispersal probability can’t be more than unity. A metapopulation with a very high dispersal probability would correspond to a well-mixed population with KN individuals and SEIR dynamics with the appropriate local rates.

2.5.2 Future applications

The derived deterministic equations can be used to investigate the models in other ways. For example, the real-time growth rate could be extracted from linearizing the dynamics around the initial state, providing an other characteristic of the dynamics that can be compared among different models. Moreover, by expanding the modified dynamics around the absence of coupling, equivalence between contact and migration might be extracted. Furthermore, additional models could be investigated analogously, like the

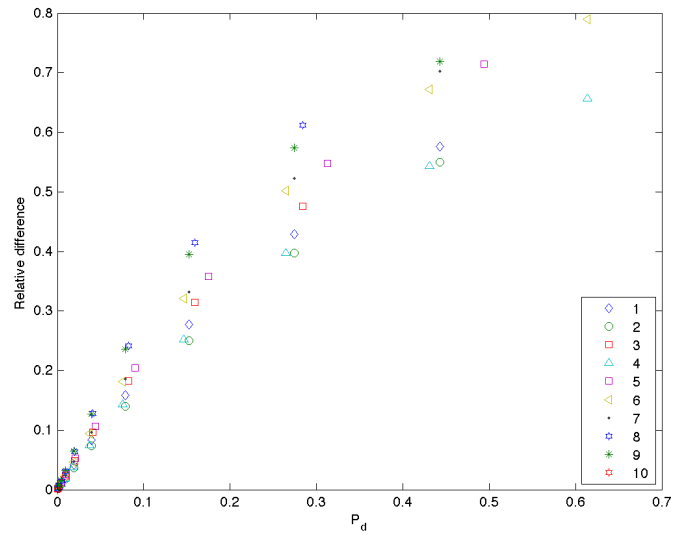


Figure 2.6: Relative difference between the basic reproductive numbers b for different parameters as a function of the dispersal probability P_d .

migration model without latency.

ID	K	λ_L	τ_E	τ_I
1	5	2	1	1
2	5	4	1	1
3	5	2	0.5	1
4	5	2	2	1
5	10	1	1	1
6	10	1	2	1
7	10	1	1	2
8	10	1	0.5	1
9	10	1	1	0.5
10	5	1	0.01	1

Table 2.5: Examined parameter sets. The values for the migration rate varied between 10^{-3} and $10^{-0.1}$, with 10 values logarithmically spaced and the global infection rate was set to $\lambda_G = \frac{m}{\tau_I(m+1/\tau_E)}$.

3

Application - DFTD

The Devil Facial Tumor Disease (DFTD) is an infectious cancer, causing a severe decline in the Tasmanian devil population, the largest surviving marsupial carnivore. The disease seems to spread independent of the population density, threatening the species with extinction [20].

3.1 Introduction

3.1.1 The Tasmanian devil

Tasmanian devils are solitary, except for females bringing up their pups. They are not territorial, living in overlapping "home ranges" instead and interacting through social feeding and during the mating season [21]. Most mating occurs seasonally, from mid-February to mid-march. After a short gestation (14–22 days), up to four young may be suckled, which emerge from the pouch in July through August and become independent of their mother by early February [22]. Devils have a lifespan of <6 years in the wild, and only a few females reproduce before 2 years of age, although an increased early reproduction have been observed in infected populations [23]. Devils are wide-spread in Tasmania, the population forming one continuous block. They are most common in the eastern and northern parts of the island (figure 3.1) [24].

Contact between tasmanian devils have been studied, with special attention to the seasonal, demographic and density-related patterns through observing social feeding [26] and using proximity sensing radio collars [27]. The resulting contact networks were not highly aggregated, but still differed slightly from random networks. A seasonal pattern was observed in the interaction among sexes: female-male interactions dominate the mating and female-female other seasons.

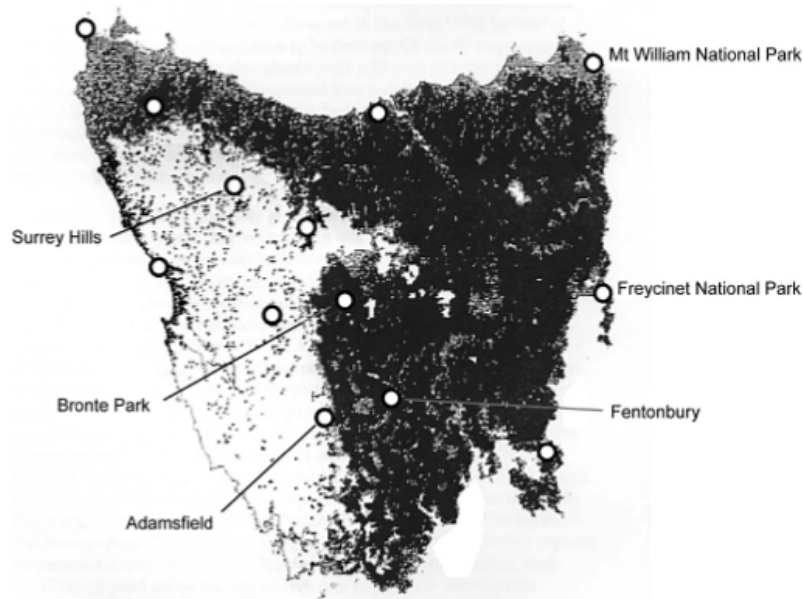


Figure 3.1: Distribution of Tasmanian devils represented as the probability of occurrence in 1 km² grid blocks, predicted by species environmental domain analysis on the basis of results from a combination of presence survey techniques [25]. Circles indicate the location of some sites trapped by the Devil Disease Project Team [24].

3.1.2 Tasmanian Devil Facial Tumour Disease (DFTD)

DFTD is an infectious cancer with a long latent period (3-9 months), leading to certain death in approximately 6 months. The disease spreads mainly through biting, with a transmission rate apparently independent of density, predicting the extinction of the species [20]. DFTD has spread over the majority of Tasmania, leading to an overall population decrease of approximately 60% and local declines up to 90% [28]. However, the population in the north-western part of Tasmania slightly differs from the rest of the population, leading to decreased susceptibility to the disease [29].

Time-series on the density of devils and the prevalence of the disease (proportion of infected animals in the population) are available from a number of sites [7], while less detailed data on population sizes is obtained through spotlighting surveys across the whole island [24] [20]. Local prevalence generally increases exponentially, reaching a constant value (see figure 3.2) with a continuously decreasing population size.

3.2 Previous models

Detailed analysis is available on the local dynamics. These models are compartmental, with susceptible (S), exposed (E) and infective (I) classes with respect to disease

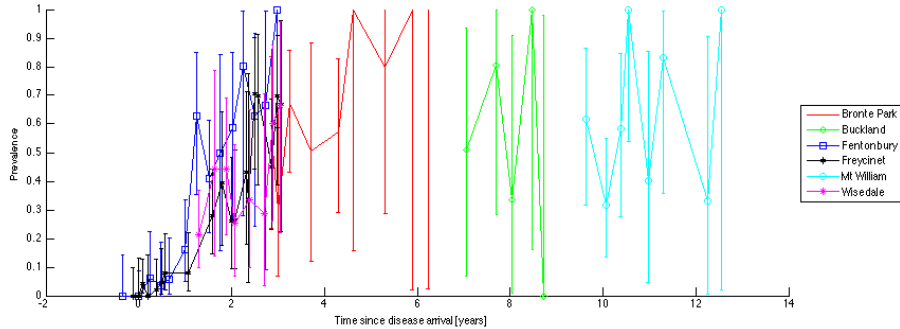


Figure 3.2: Estimated prevalence from mark-recapture analysis at all monitored sites with 95% confidence intervals, as a function of time since (estimated) disease arrival. Data from [7].

dynamics. Since the time-scale of the disease is in the same range as the devil’s life-time, demography can’t be neglected. The demography of the devil is included through age-classes and birth- and death rates according to the logistic growth model.

Most of the previous models are deterministic and well-mixed. A simple model with exponential transfer times have been used to estimate parameters and show that a frequency-dependent transmission rate is more appropriate to describe the disease dynamics than a density dependent one, since prevalence from field data appears to remain high even for significantly decreased population sizes [7].

A similar model, generalized to incorporate gamma-distributed delays have been used to estimate the effects of a possible control measure, culling. It has been found, that unrealistically effective efforts are needed for success, in agreement with the inefficiency of a culling trial on one of the sites in Tasmania. Immigration from sites unaffected by culling probably worsens the model predictions even more. A fundamentally different model, using delay differential equations gave similar conclusions [30].

Lastly, a stochastic model was used to investigate the effect of heterogeneity in contact patterns. Disease was simulated on a contact network empirically derived, using data collected by proximity sensors. The result was, that the network structure changed the probabilities for the different outcomes, but hardly changed the reproductive numbers [31].

3.3 My spatial model

The model I constructed is a stochastic, individual-based, spatially explicit model incorporating age-structure and continuous in time. I used 5 age classes and demographic parameters as estimated from current knowledge of devil life history and some basic modelling in [30]. In order to simplify the model and minimize the number of parameters, I used exponentially distributed delays both for the latent period and for aging. I

Process	Rate	Effects
Birth	$\sum_{\alpha} b_{\alpha} N_i^{\alpha} (1 - N/K)$	$S_i^1 \rightarrow S_i^1 + 1$
Aging of type X , age class α	X_i^{α}	$X_i^{\alpha} \rightarrow X_i^{\alpha} - 1, X_i^{\alpha+1} \rightarrow X_i^{\alpha+1} + 1$
Death of type X , age class α	$d^{\alpha} X_i^{\alpha}$	$X_i^{\alpha} \rightarrow X_i^{\alpha} - 1$
Infection from age class α to β	$\frac{1}{N_i} (I_i^{\alpha} + c \sum_{j \in NN} I_j^{\alpha}) \eta_{\alpha}^{\beta} S_i^{\beta}$	$S_i^{\alpha} \rightarrow S_i^{\alpha} - 1, E_i^{\alpha} \rightarrow E_i^{\alpha} + 1$
Outbreak in age class α	$\frac{1}{\tau_E} E_i^{\alpha}$	$E_i^{\alpha} \rightarrow E_i^{\alpha} - 1, I_i^{\alpha} \rightarrow I_i^{\alpha} + 1$
DFTD-associated death in age class α	$\frac{1}{\tau_I} I_i^{\alpha}$	$I_i^{\alpha} \rightarrow I_i^{\alpha} - 1$
Migration from patch i to j	$\frac{\mu_{\alpha}}{N_h} X_i^{\alpha}$	$X_i^{\alpha} \rightarrow X_i^{\alpha} - 1, X_j^{\alpha} \rightarrow X_j^{\alpha} + 1$

Table 3.1: Rates and effects of possible events in the spatial model of DFTD. Compartments: S -susceptible, E -exposed and I -infected, while $N = S + E + I$ denotes the population size. Latin characters index patches and greek letters the N_a age classes. $\eta_{\alpha\beta}$ is an N_a by N_a constant matrix, b_{α} , d_{α} and m_{α} are N_a long constant vectors and τ_E and τ_I are constants

assumed the transmission rate to be frequency-dependent.

Spatial structure I placed a grid on the island of Tasmania, each cell corresponding to a population in my metapopulation model. Carrying capacities were set to be proportional with the average devil density on the site from [24] and the total population was set approximately to 140.000 in order to match informal estimates of the total healthy tasmanian devil population of 130.000-150.000 individuals [20].

Between-patch interactions Coupling between patches was realized in two ways. First, individuals were allowed to migrate, corresponding to permanently moving away. Migration was assumed to be instantaneous and the new site was chosen uniformly randomly among all hospitable ($K > 0$) nearest neighbour sites. The age-class dependent rate μ_{β} was constant (m) per adult animal and zero for juveniles, since they spend most of their times in the den with their mother.

Second, individuals on neighbouring patches were allowed to interact and possibly infect each other. This kind of contact originates from the overlap between home-ranges of animals on different, neighbouring patches. Infectives of neighbouring patches were considered as candidates for infecting susceptibles, with their effect damped by a constant factor c (see the resulting rate in table 3.1).

Initialization All patches were initialized with an age-distribution according to the fixed point of my local demographic model's deterministic version, age-structured demography with logistic growth. The definition of the model and its fixed points are shown on figure 3.3. To start the infection, a small proportion of the population on the initial case's site was turned infective.

$$\begin{aligned}
\frac{dN_1}{dt} &= \sum_{i=1}^k b_i N_i (1 - \sum_{i=1}^k N_i) - (1 + d_1) N_1 & N_1^* &= \frac{\sum_i b_i \alpha_i^{-1-d_1}}{(\sum_j \alpha_j) \sum_i b_i \alpha_i} & \alpha_1 &= 1 \\
\frac{dN_i}{dt} &= N_{i-1} - (1 + d_i) N_i & N_i^* &= \alpha_i N_1 & \alpha_i &= \frac{\alpha_{i-1}}{1+d_i} \\
\frac{dN_k}{dt} &= N_{k-1} - d_k N_k & & & \alpha_k &= \frac{\alpha_{k-1}}{d_k}
\end{aligned}$$

Figure 3.3: Left: deterministic age-structured model with logistic growth. Middle, right: fixed point of the model. Latin characters index age cohorts.

3.4 Fitting the model

My first task was to fit the model to the data and investigate whether it can capture all main aspects of the real-life disease dynamics.

3.4.1 Parameters to fit

I used the local, age-dependent birth rate and death rate as estimated in [30]. Moreover, I used the infection matrix $\eta_{\alpha,\beta}$ up to a constant factor, that I will call infection rate, from the same article. Besides the two parameters describing the spatial spread, the migration rate and the between-patch contact rate, this leaves two local parameters to fit. The latent period was not well-known due to the lack of diagnostic tools capable of diagnosing the disease before the visible signs. The infection rate in previous models was determined to fit the initial increase in prevalence, so I had to fit it again to take the effect of other patches into account.

Indirect data on the migration rate was available through the apparent yearly survival rates, consisting of natural death and emigration. I scaled the apparent yearly survival rates from [28] to match the median life expectancy of devils (the same procedure as in [30]). Then, since these rates consist of death and emigration, rest of the rates, not explained by natural death, could be considered as the migration rate.

3.4.2 Response variables

I choose four simple characteristics of the disease dynamics for quantifying the agreement between my simulation and field data. Firstly, for the short-term, local dynamics, I used the initial increase in adult prevalence, determining the speed of the local spread. Secondly, for the long-term local behaviour, I focused on the equilibrated value of prevalence in adults. Finally, to characterize the spatial spreading, I chose the speed of the disease front.

Initial increase in adult prevalence

The rate of initial increase in adult prevalence is the increase in the proportion of infected and exposed individuals in the population per unit of time, on a logarithmic scale, excluding the first age class. This quantity is often denoted as r_0 .

From the data, I considered only a single site, Fentonbury, since all other sites were problematic (e.g. late start of monitoring, spatial structure, participation in a culling trial, special genetics). r_0 for this site is estimated to be 2.2644, with 95% confidence interval [1.4663, 3.1208], derived from Highest Posterior Density intervals from a Markov chain Monte Carlo sample (n=50000 iterations) in [7].

As for the simulations, I recorded the adult prevalence on all sites. I considered central, large sites, similar to Fentonbury, and determined r_0 from a linear fit after a logarithmic transformation of the initial phase of the disease (figure 3.4). Finally, I averaged for sites yielding a good fit ($R^2 > 0.8$), checking that most sites resulted in good fits.

Equilibrial prevalence

According to the data, the long-term local behaviour is characterized by a constantly decreasing population size with an approximately constant prevalence, in agreement with a frequency-dependent transmission rate. In order to determine this equilibrial value from the data, I considered sites where the disease has long been established (for at least 10 years): Mount Williams, the site where the first case was observed, Bronte Park and Buckland. Confidence intervals were large but there was hardly any evidence for a trend in time (low correlations with time). Moreover, the mean long-term prevalence did not differ significantly between sites, based on a one-way ANOVA test. The mean of all data points was 0.6424 with a 95% confidence interval of [0.5203, 0.7644].

In the simulations, I averaged for a time-range based on r_0 , in order to avoid taking the initial transient into account, but also keep the effects of strong fluctuations due to low population size and/or prevalence in very early and very late phases low. I used data from $5/r_0$ to $15/r_0$ after the establishment of the disease, defined as the point where the number of diseased animals reached 5 (figure 3.4).

Speed of the disease front

Last, for the spatial spread, I chose the speed of the travelling wave of infection, the disease front. Field data consisted only of a few points, since the front could not be monitored closely. Moreover, the distance of documented cases from the initial case appears to be random, but this is only due to the increased publicity of the epidemic: the number of reports increased drastically after 2003, but they were mostly from already diseased, but not yet monitored sites.

However, if we consider only the case at maximal distance in each year, the data points fall on a line. This approach is especially useful since it masks inhomogeneities that my model with homogeneous contacts could not and did not attempt to capture. I modified the time and location of the initial case for the data in order to achieve a better fit, since the exact values are not well-known. All reports and the result of the fit are shown on figure 3.5. The resulting estimation for the speed of the disease front is 25.8081, with a 95% confidence interval of [17.2490, 34.3671].

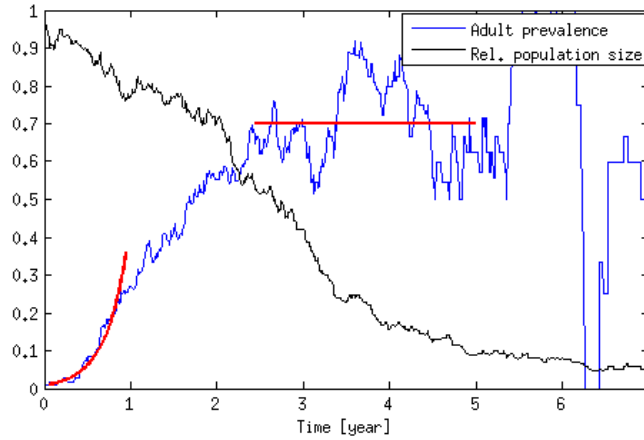


Figure 3.4: Typical time-series from a single site in my spatially explicit, stochastic simulation. Red lines illustrate the results of fitting for the initial increase in prevalence and equilibrium prevalence.

The wave of infection was also clearly visible on my simulation (figure 3.6). The maximal distance from the initial site to the disease front was recorded 100 times a year and a linear fit was performed for the "middle" part of the spread (from 1/6 up to 3/4 times the maximal distance) in order to avoid strong fluctuations during establishment and finite-size effects towards reaching the edge of the island (figure 3.7). Results were considered to be in agreement with the data, if the slope of the fit was within the 95% confidence interval of the estimation from the data.

3.4.3 Results

First, I considered the case without migration. However, the resulting population was highly susceptible to stochastic fluctuations, leading to extinctions in smaller patches. Next, I set the contact rate to zero, considering migration only. In this case, however, a very high migration rate was needed for the speed of the disease front to match the data: average adult individuals were supposed to change patches once a year, more than one would suppose from the rate of 0.584, as estimated from the data.

Finally, I considered the general case of both migration and contact. I investigated three, realistic values of latent periods (3 months, 6 months and 9 months) and performed a full parameter search on the other three input parameters (local infection rate, between-patch contact rate and migration rate). Example results for a fixed latent period of 6 months are shown on figure 3.8.

We can observe that the effect of migration on the local dynamics is small compared to that of contact, due to the increased infection pressure coming from neighbouring patches through contact (first row on figure 3.8). Moreover, an unrealistically large migration rate (above 1) results in irregular dynamics that cannot be characterized by

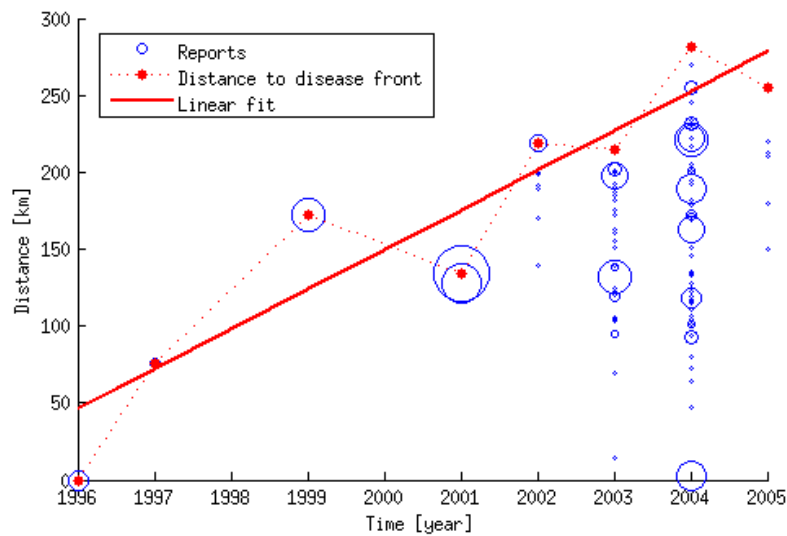


Figure 3.5: Spatial spread of DFTD. Blue circles: all reports on diseased animals from Tasmania with the sizes of circles proportional to the number of infected animals reported. Red diamonds: cases at maximal distance from the initial case in each year. Red line: result of a linear fit.

these output parameters.

We can also learn from these figures, that there is a parameter range where my simulation captures all of the above described characteristics of the dynamics and thus can be used to model the spatial spreading of devil facial tumour disease.

3.5 Future work

Next, I will use the model with parameters where it describes the dynamics of DFTD in applications. For instance, it can be used to make predictions about the global outcome of the epidemic. To the local model, only three outcomes are possible: host extinction, disease extinction or disease-host coexistence, the last one not relevant in the case of DFTD, due to density-dependent transmission. However, the spatial dimension also allows a spatially inhomogeneous disease-host coexistence, where patches eradicated by the disease can recover and be infected again, while the epidemic travels around the island.

Furthermore, possible control measures could be modelled. For instance, culling (the removal of infective individuals) or influencing the coupling strength (e.g. through construction of fences or artificially transporting individuals) could be investigated in a spatial context.

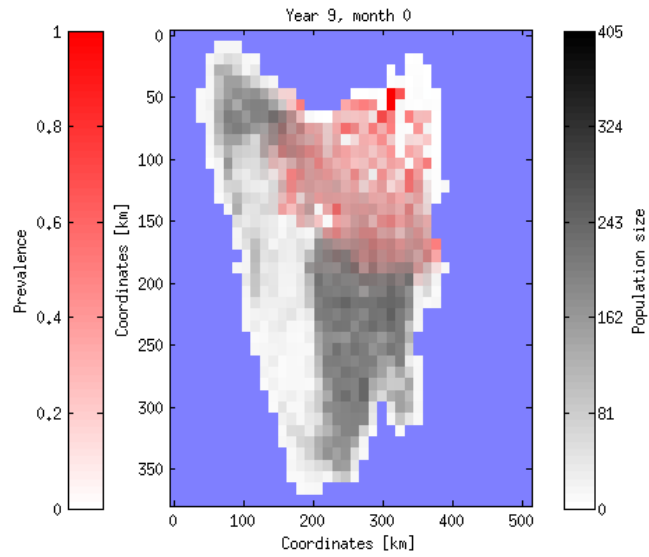


Figure 3.6: Snapshot of the spatial simulation with a clearly visible disease front.

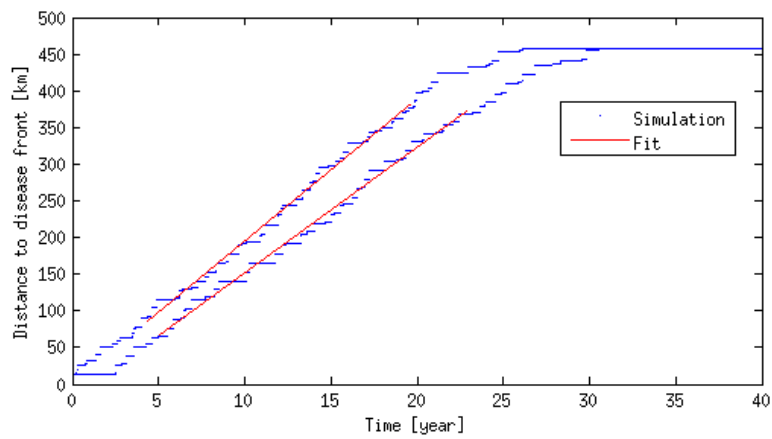


Figure 3.7: Typical simulation results for the speed of the disease front.

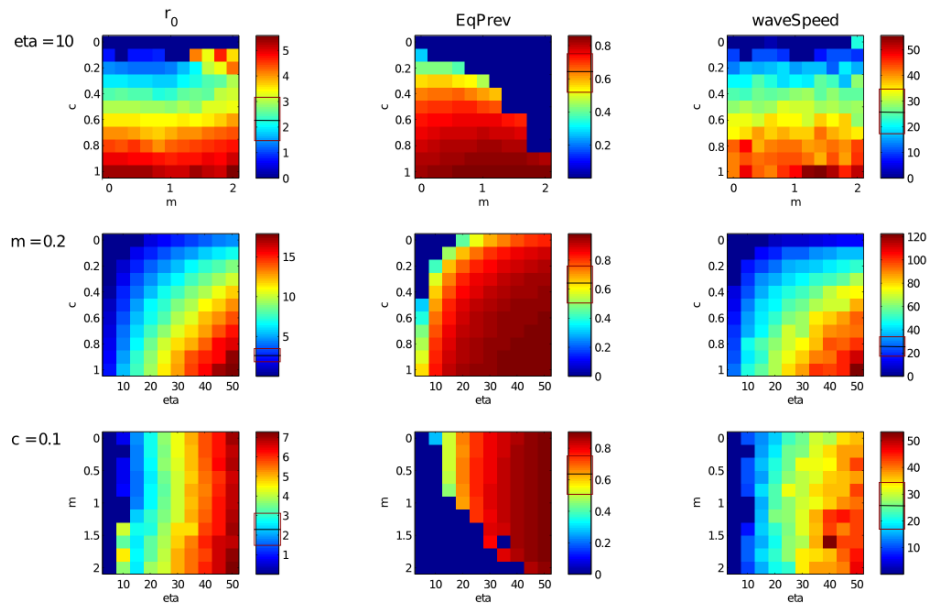


Figure 3.8: The output parameters as a function of pairs of input parameters for a latent period $\tau_E = 6$ months. r_0 : rate of initial increase in prevalence, $eqPrev$: equilibril value of prevalence and $waveSpeed$: speed of the disease front ([km/year]). A lack of local/spatial spread is denoted by zero outputs. Parameters estimated from data are marked on the colorbars (black: estimation, red: 95% confidence interval).

Bibliography

- [1] P. C. Cross, P. L. F. Johnson, J. O. Lloyd-Smith, W. M. Getz, Utility of R_0 as a predictor of disease invasion in structured populations, *JOURNAL OF THE ROYAL SOCIETY INTERFACE* 4 (13) (2007) 315–324.
- [2] M. Jesse, P. Ezanno, S. Davis, J. A. P. Heesterbeek, A fully coupled, mechanistic model for infectious disease dynamics in a metapopulation: Movement and epidemic duration, *JOURNAL OF THEORETICAL BIOLOGY* 254 (2) (2008) 331–338.
- [3] A. Kamenev, B. Meerson, Extinction of an infectious disease: A large fluctuation in a nonequilibrium system, *PHYS. REV. E* 77 (2008) 061107.
URL <http://link.aps.org/doi/10.1103/PhysRevE.77.061107>
- [4] B. Grenfell, B. Bolker, Cities and villages: infection hierarchies in a measles metapopulation, *ECOLOGY LETTERS* 1 (1) (1998) 63–70.
- [5] M. I. Dykman, I. B. Schwartz, A. S. Landsman, Disease extinction in the presence of random vaccination, *PHYS. REV. LETT.* 101 (2008) 078101.
URL <http://link.aps.org/doi/10.1103/PhysRevLett.101.078101>
- [6] P. v. d. D. Fred Brauer, J. Wu (Eds.), *Mathematical Epidemiology*, Vol. 1945 of *Lecture Notes in Mathematics*, Springer Berlin Heidelberg, 2008.
- [7] H. McCallum, M. Jones, C. Hawkins, R. Hamede, S. Lachish, D. L. Sinn, N. Beeton, B. Lazenby, Transmission dynamics of tasmanian devil facial tumor disease may lead to disease-induced extinction, *Ecology* 90 (12) (2009) 3379–3392.
URL <http://www.esajournals.org/doi/abs/10.1890/08-1763.1>
- [8] F. Ball, M. Dennis, G. Scalia-Tomba, Epidemics with two levels of mixing, *ANNALS OF APPLIED PROBABILITY* 1 (1) (1997) 46–89.
- [9] F. Ball, P. Neal, A general model for stochastic SIR epidemics with two levels of mixing, *MATHEMATICAL BIOSCIENCES* 180 (SI) (2002) 73–102.

- [10] B. BOLKER, B. GRENFELL, Space, persistence and dynamics of measles epidemics, *PHILOSOPHICAL TRANSACTIONS OF THE ROYAL SOCIETY OF LONDON SERIES B-BIOLOGICAL SCIENCES* 348 (1325) (1995) 309–320.
- [11] J. V. Ross, T. House, M. J. Keeling, Calculation of Disease Dynamics in a Population of Households, *PLOS ONE* 5 (3).
- [12] P. Cross, J. Lloyd-Smith, P. Johnson, W. Getz, Duelling timescales of host movement and disease recovery determine invasion of disease in structured populations, *ECOLOGY LETTERS* 8 (6) (2005) 587–595.
- [13] V. Colizza, A. Vespignani, Epidemic modeling in metapopulation systems with heterogeneous coupling pattern: Theory and simulations, *JOURNAL OF THEORETICAL BIOLOGY* 251 (3) (2008) 450–467.
- [14] M. Keeling, P. Rohani, Estimating spatial coupling in epidemiological systems: a mechanistic approach, *ECOLOGY LETTERS* 5 (1) (2002) 20–29.
- [15] A. Vazquez, Epidemic outbreaks on structured populations, *JOURNAL OF THEORETICAL BIOLOGY* 245 (1) (2007) 125–129.
- [16] A. Park, S. Gubbins, C. Gilligan, Extinction times for closed epidemics: the effects of host spatial structure, *ECOLOGY LETTERS* 5 (6) (2002) 747–755.
- [17] L. Pellis, F. Ball, P. Trapman, Reproduction numbers for epidemic models with households and other social structures. I. Definition and calculation of R_0 , *MATHEMATICAL BIOSCIENCES* 235 (1) (2012) 85–97.
- [18] F. Ball, P. D. O’Neill, J. Pike, Stochastic epidemic models in structured populations featuring dynamic vaccination and isolation, *JOURNAL OF APPLIED PROBABILITY* 44 (3) (2007) 571–585.
- [19] L. Pellis, N. M. Ferguson, C. Fraser, Epidemic growth rate and household reproduction number in communities of households, schools and workplaces, *JOURNAL OF MATHEMATICAL BIOLOGY* 63 (4) (2011) 691–734.
- [20] H. McCallum, D. M. Tompkins, M. Jones, S. Lachish, S. Marvanek, B. Lazenby, G. Hocking, J. Wiersma, C. E. Hawkins, Distribution and impacts of tasmanian devil facial tumor disease, *EcoHealth* 4 (3) (2007) 318–325.
URL <http://link.springer.com/article/10.1007/s10393-007-0118-0>
- [21] E. Guiler, Observations on the tasmanian devil, *sarcophilus harrisii* (marsupialia : Dasyuridae) i. numbers, home, range, movements and food in two populations., *Australian Journal of Zoology* 18 (1) (1970) 49–62.
- [22] H. Hesterman, S. Jones, F. Schwarzenberger, Reproductive endocrinology of the largest dasyurids: Characterization of ovarian cycles by plasma and fecal steroid monitoring. part i. the tasmanian devil (*sarcophilus harrisii*), *General and*

- Comparative Endocrinology 155 (1) (2008) 234 – 244.
URL <http://www.sciencedirect.com/science/article/pii/S0016648007001864>
- [23] M. E. Jones, A. Cockburn, R. Hamede, C. Hawkins, H. Hesterman, S. Lachish, D. Mann, H. McCallum, D. Pemberton, Life-history change in disease-ravaged tasmanian devil populations, *Proceedings of the National Academy of Sciences* 105 (29) (2008) 10023–10027.
URL <http://www.pnas.org/content/105/29/10023>
- [24] C. Hawkins, C. Baars, H. Hesterman, G. Hocking, M. Jones, B. Lazenby, D. Mann, N. Mooney, D. Pemberton, S. Pyecroft, M. Restani, J. Wiersma, Emerging disease and population decline of an island endemic, the tasmanian devil *sarcophilus harrisii*, *Biological Conservation* 131 (2) (2006) 307–324.
URL <http://www.sciencedirect.com/science/article/pii/S0006320706001595>
- [25] M. Jones, R. Rose, Preliminary assessment of distribution and habitat associations of spotted-tailed quoll (*dasyurus maculatus*) and eastern quoll (*d. viverrinus*) in tasmania to determine conservation and reservation status, Parks and Wildlife Service Tasmania: Report to Tasmanian Regional Forest Agreement Environment and Heritage Technical Committee.
- [26] R. K. Hamede, H. McCallum, M. Jones, Seasonal, demographic and density-related patterns of contact between tasmanian devils (*sarcophilus harrisii*): Implications for transmission of devil facial tumour disease, *Austral Ecology* 33 (5) (2008) 614–622.
URL <http://onlinelibrary.wiley.com/doi/10.1111/j.1442-9993.2007.01827.x/abstract>
- [27] R. K. Hamede, J. Bashford, H. McCallum, M. Jones, Contact networks in a wild tasmanian devil (*sarcophilus harrisii*) population: using social network analysis to reveal seasonal variability in social behaviour and its implications for transmission of devil facial tumour disease, *Ecology Letters* 12 (11) (2009) 1147–1157.
URL <http://onlinelibrary.wiley.com/doi/10.1111/j.1461-0248.2009.01370.x/abstract>
- [28] S. Lachish, M. Jones, H. McCallum, The impact of disease on the survival and population growth rate of the tasmanian devil, *Journal of Animal Ecology* 76 (5) (2007) 926–936.
- [29] R. Hamede, S. Lachish, K. Belov, G. Woods, A. Kreiss, A. PEARSE, B. Lazenby, M. Jones, H. McCALLUM, Reduced effect of tasmanian devil facial tumor disease at the disease front, *Conservation Biology* 26 (1) (2012) 124–134.

- [30] N. Beeton, H. McCallum, Models predict that culling is not a feasible strategy to prevent extinction of tasmanian devils from facial tumour disease, *Journal of Applied Ecology* 48 (6) (2011) 1315–1323.
- [31] R. Hamede, J. Bashford, M. Jones, H. McCallum, Simulating devil facial tumour disease outbreaks across empirically derived contact networks, *Journal of Applied Ecology* 49 (2) (2012) 447–456.
URL <http://onlinelibrary.wiley.com/doi/10.1111/j.1365-2664.2011.02103.x/abstract>
- [32] A. Eriksson, F. Elías-Wolff, B. Mehlig, Metapopulation dynamics on the brink of extinction, *Theoretical population biology*.

A

Local model

A.1 SEIR model and its deterministic approximation

I investigate the local SEIR dynamics in this section in order to verify the local dynamics of the patches in my model before connecting them into a metapopulation. The model consists of four compartments: susceptible (S), exposed (E), infected (I) and recovered (R) individuals in a well-mixed population. The following transitions are possible between the types: $S \rightarrow E$ (infection), $E \rightarrow I$ (outbreak) and $I \rightarrow R$ (recovery), with rates according to the law of mass action (figure A.1).

The following deterministic approximation is precise for an infinite population:

$$\begin{aligned}\dot{S} &= -\eta SI, \\ \dot{E} &= \eta SI - \tau_E^{-1} E, \\ \dot{I} &= \tau_E^{-1} E - \tau_I^{-1} I, \\ \dot{R} &= \tau_I^{-1} I.\end{aligned}\tag{A.1}$$

Consequentially, $S + E + I + R = K$, where K is the constant population size. As a result, the difference between the density-dependent (ηSI) and the density-independent rates ($\eta SI/K$) is a constant factor. I will continue to use the notation for the density-dependent case.

The fraction of individuals unaffected by the disease can be approximated from the deterministic model, assuming the initial conditions $E_0 = I_0 = R_0 = 0$, $K = S_0$. From equation (A.1),

$$\frac{\dot{S}}{S} = -\eta I = -\eta \tau_I \dot{R} \equiv -R_0 \dot{R}\tag{A.2}$$

resulting in

$$S(t) = S_0 e^{-\eta \tau_I R(t)}.\tag{A.3}$$

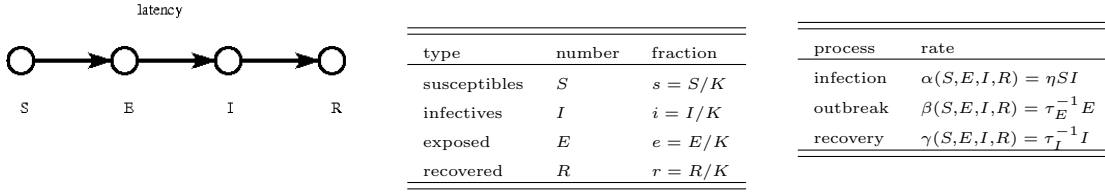


Figure A.1: Left: local SEIR model. Middle: susceptibles S , exposed (or latent) E , infectives I , recovered R . Right: rates in stochastic model.

Since $E(\infty) = I(\infty) = 0$, this implies $S(\infty) = S_0 \exp[-\eta\tau_I(K - S(\infty))]$ and thus

$$x = e^{-R_0(1-x)} \quad (\text{A.4})$$

where $x = S(\infty)/S_0$ is the fraction of individuals unaffected by the disease, and $R_0 = \eta\tau_I S_0$ is the reproductive value of the infection. The above result also means that latency has no effect upon x .

A.2 Stochastic simulations

First, I computed the final fraction of susceptibles by stochastic simulations and compared my results to the prediction of the deterministic approximation (A.4). I used the initial condition $E_0 = 1$ in order to be closest to the assumption $K = S_0$. However, this made the system extremely sensitive to stochastic fluctuations in the early stages of an epidemic, where the number of individuals effected is still low. In order to avoid taking cases with premature extinction due to stochasticity into account, I only considered cases with a "large" outbreak by discarding all runs with less than $K/4$ individuals effected.

I simulated several epidemics, measuring x and the fraction of runs discarded, F . The distribution of x for certain parameters with R_0 not too close to unity can be seen on figure A.2. A sharp peak at $x = 1$ (no individuals affected) can be observed runsfor the unconditional case, corresponding to the premature extinction of the epidemy, as mentioned above. This peak - trivially - is missing in the conditional case, since it cuts the distribution at $x = 0.75$. Also, the mean with the condition is relatively close to the theoretical value for $K \rightarrow \infty$, but without the condition, the distribution is strongly biased towards $x = 1$, resulting in a significantly larger mean.

Next, I varied the parameters K , η , τ_E and τ_I , measuring the mean value of x conditional on an outbreak. I investigated the effect of varying a single parameter, while keeping the other three fixed. My results can be seen on figures A.4 and A.3. We can observe, that x depends only on $R_0 = \eta\tau_I S_0$, according to (A.4) and is independent of τ_E .

Afterwards, I considered the fraction of runs discarded, F (figure A.3). The simulations agreed with the prediction $F \approx 1 - 1/R_0$ provided that R_0 was not too close to unity.

Finally, I reduced the population size K while keeping $R_0 = 2$ fixed and computed the distribution and mean value of x (figure A.5). The distribution becomes sharper

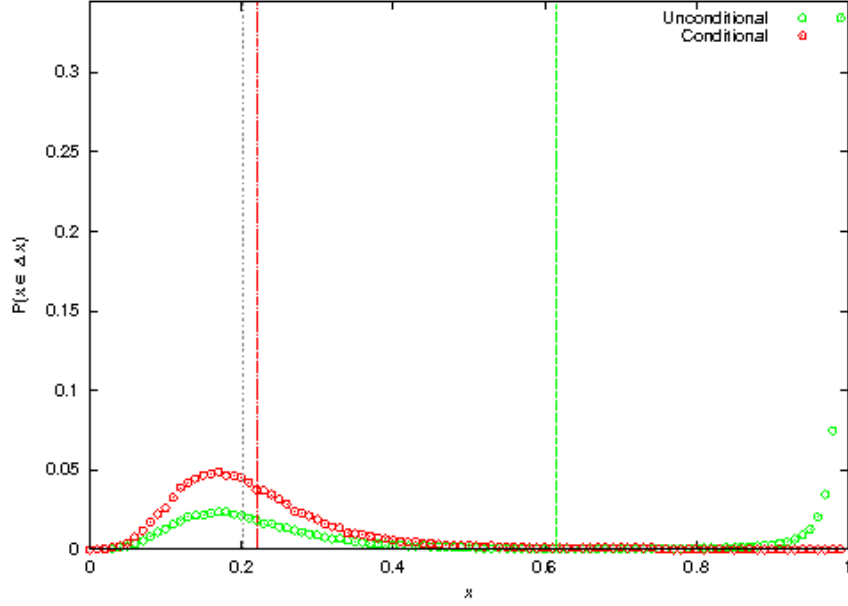


Figure A.2: Distribution of x for $K = 100$, $\eta = 0.005$, $\tau_I = 4$, $\tau_E = 1$ with conditional and unconditional on an outbreak. Horizontal lines mark the theoretical value of x from the deterministic model (grey) and the means of the distributions (red and green, respectively).

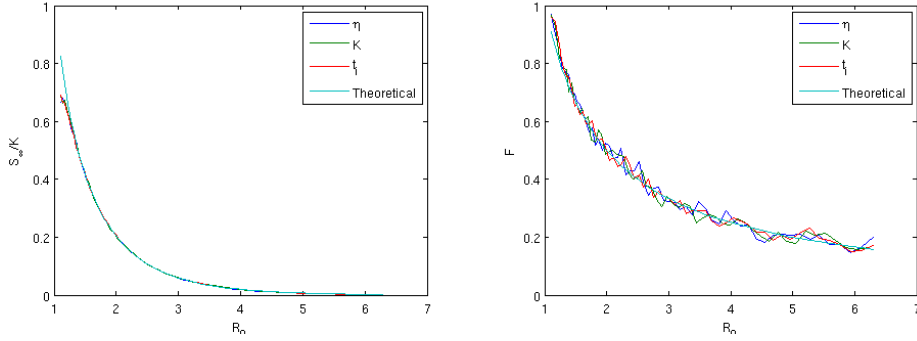


Figure A.3: Fraction of susceptibles left after epidemy and fraction of cases without epidemy as a function of $R_0 = \eta\tau_I S_0$. Average over 500 runs.

as K increases, since fluctuations become less significant. Moreover, the mean value of x approaches the theoretical value for $K \rightarrow \infty$ from higher values, corresponding to a tendency of downward fluctuations for smaller population sizes.

The agreement of the results both for x and F with the theoretical results show that the local dynamics in my stochastic simulations indeed correctly model disease spreading.

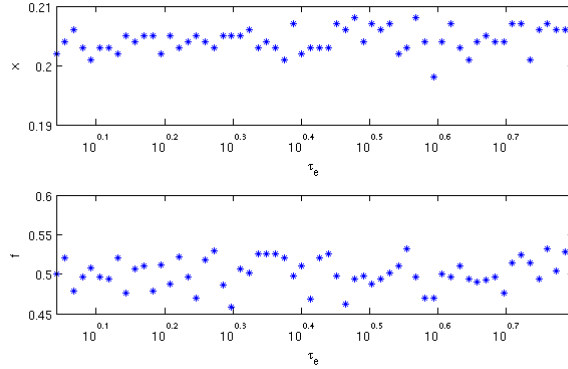


Figure A.4: Fraction of susceptibles left after epidemic and fraction of cases without epidemic for $R_0 = 2$ and several values of τ_E . Average over 500 runs. $\Delta x/x \approx 1\%$, $\Delta f/f \approx 3.7\%$ ($1/\text{sqrt}(500) \approx 4\%$)

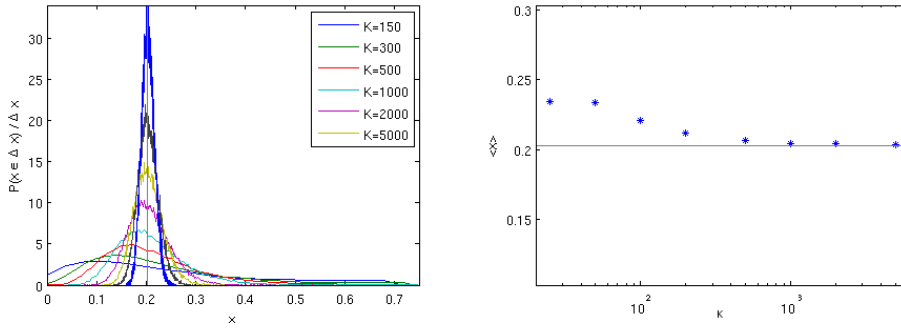


Figure A.5: Distribution and mean value of x for different K , $R_0 = 2$, 500 simulations.

A.3 Master equation

The local, stochastic SEIR model can also be described in terms of a master equation. The master equation is the differential equation determining the evolution of $\rho_{S,E,I}$, the probability that the population is in the state (S,E,I) : S susceptible, E exposed, I infected and $R = K - S - E - I$ recovered individuals.

Every process in the population (infection, outbreak and recovery) contributes with two terms: a positive for the population reaching the state and a negative for leaving it. For example, the change in ρ under an infinitesimal time interval Δt due to infection is the following: $\alpha_{S+1,E-1,I}\rho_{S+1,E-1,I}\Delta t - \alpha_{S,E,I}\rho_{S,E,I}\Delta t$, while contributions from other processes can be computed similarly. After summing all terms, the following master

equation is obtained:

$$\begin{aligned} \frac{d\rho_{S,E,I}}{dt} = & \alpha_{S+1,E-1,I}\rho_{S+1,E-1,I} + \beta_{S,E+1,I-1}\rho_{S,E+1,I-1} + \\ & \gamma_{S,E,I+1}\rho_{S,E,I+1} - (\alpha_{S,E,I} + \beta_{S,E,I} + \gamma_{S,E,I})\rho_{S,E,I} \end{aligned} \quad (\text{A.5})$$

A.4 Limit of infinite population

In order to derive the deterministic equation (A.1) from the master equation, we can expand it in $1/K$ and take the limit of $K \rightarrow \infty$. First, we introduce new variables: $s = S = K$, $e = E/K$ and $i = I/K$ and functions $\alpha_{S,E,I} = K\alpha(s,e,i)$, $\beta_{S,E,I} = K\beta(s,e,i)$, $\gamma_{S,E,I} = K\gamma(s,e,i)$ and $\rho(s,e,i) = \rho_{S,E,I}$.

The master equation can be formulated easier by introducing the following operator, acting on a continuous function of s , e and i and expressing it in terms of derivatives:

$$E_s^\pm g(s,e,i) = g(s \pm 1/K, e, i) = \sum_{k=0}^{\infty} \frac{(\pm 1/K)^k}{k!} \frac{\partial^k g}{\partial s^k} = e^{\pm \frac{d}{K ds}} g(s,e,i) \quad (\text{A.6})$$

E_e^\pm and E_i^\pm are defined analogously.

Using the above definitions, the master equation can be reformulated as

$$\begin{aligned} \frac{d\rho(s,e,i)}{dt} = & (E_s^+ E_e^- - 1) K\alpha(s,e,i)\rho(s,e,i) + \\ & (E_e^+ E_i^- - 1) K\beta(s,e,i)\rho(s,e,i) + \\ & (E_i^+ - 1) K\gamma(s,e,i)\rho(s,e,i) \end{aligned} \quad (\text{A.7})$$

In the limit of $K \rightarrow \infty$, the above equation takes the form of a transport equation for s , e and i , since the operators can be expanded in $1/K$. For example the first term is

$$E_s^+ E_e^- - 1 = e^{\frac{d}{K ds} - \frac{d}{K de}} - 1 \rightarrow \left(\frac{d}{ds} - \frac{d}{de} \right) / K \quad (\text{A.8})$$

After expanding all terms and considering an infinite population, the following form can be obtained:

$$\frac{d\rho}{dt} = -\nabla(\underline{v}\rho) \quad (\text{A.9})$$

where

$$\nabla = \left[\frac{d}{ds}, \frac{d}{de}, \frac{d}{di} \right] \quad (\text{A.10})$$

and

$$\underline{v} = [-\alpha, \alpha - \beta, \beta - \gamma] \quad (\text{A.11})$$

corresponding to the following, deterministic equation:

$$\begin{aligned} \dot{s} &= -\alpha(s,e,i), \\ \dot{e} &= \alpha - \beta(s,e,i), \\ \dot{i} &= \beta - \gamma(s,e,i), \\ r &= 1 - s - e - i, \end{aligned} \quad (\text{A.12})$$

equivalent to (A.1) since $\alpha = \eta si$, $\beta = e/\tau_E$ and $\gamma = i/\tau_I$.

B

Standard metapopulation

B.1 Introduction

In this chapter, I investigated the standard metapopulation model with birth, death and migration as described in [32]. I used the theoretical results from this article to verify my metapopulation model before applying its modified version for disease spreading.

The stochastic, individual-based model consists of N patches, with local dynamics according to the logistic growth law, formulated through the following birth and death rates b and d , respectively

$$\begin{aligned} b_i &= ri, \\ d_i &= \mu i + (r - \mu)i^2/K, \end{aligned} \tag{B.1}$$

where i denotes the population size in a given patch, r the per capita birth rate, μ the density-independent per capita mortality, and K the carrying capacity of a single patch. For simplicity, we assume that $\mu = 1$ from now on, corresponding to measuring time in units of the expected life-time of individuals in the absence of density dependence.

Patches are coupled by migration in the standard model. In the simplest case that I investigate, individuals migrate independently, with a constant rate m , corresponding to the following emigration rate:

$$m_i = mi \tag{B.2}$$

Furthermore, I now consider homogeneous, instantaneous migration: emigrants appear at a randomly chosen patch.

B.2 Deterministic dynamics

In the limit of infinitely many patches, the stochastic dynamics become deterministic. If we denote the fraction of patches with a population size i by f_i , the following deter-

ministic dynamics can be obtained:

$$\frac{df}{dt} = \underline{v}(f) \tag{B.3}$$

where

$$\begin{aligned} v_j &= (b_{j-1} + I)f_{j-1} + (d_{j+1} + m_{j+1})f_{j+1}, \\ &\quad - (b_j + I + d_j + m_j)f_j \quad \text{for } j > 1, \\ v_1 &= I(1 - \sum_{k=1}^{\infty} f_k) + (d_2 + m_2)f_2 - (b_1 + I + d_1 + m_1)f_1. \end{aligned} \tag{B.4}$$

Here $I = \sum_{k=1}^{\infty} m_k f_k$ is the rate of immigration into a given patch and $f_0 = 1 - \sum_{k=1}^{\infty} f_k$ the normalizing factor.

In this limit, the population may persist if there exists a stable steady state \underline{f}^* such that it has a positive component $f_j^* > 0$ for some $j < 0$. It can be shown that, for a sufficiently large migration rate, the steady state $\underline{f}^* = \underline{0}$, corresponding to extinction, becomes unstable while a second steady state, determined by the following equation, emerges:

$$f_j^* = f_0 \prod_{k=1}^j \frac{b_{k-1} + I^*}{d_k + m_k} \tag{B.5}$$

where

$$I^* = \sum_{k=1}^{\infty} m_k f_k^* \tag{B.6}$$

is the rate of immigration in the steady state. It can be shown that this steady state is stable when $I^* > 0$. [32]

B.3 Comparison of distributions

First, I numerically integrated the deterministic dynamics (B.3) using Euler’s method. Next, I performed stochastic simulations to determine the distribution using rates as defined in (B.1) and (B.2). Finally, I solved equation (B.5) numerically, by a fixed-point iteration. The resulting steady-state distributions for two example parameter sets are shown on figures B.1 and B.2.

Distributions from the different methods show agreement, implying that my simulations correctly model a standard metapopulation.

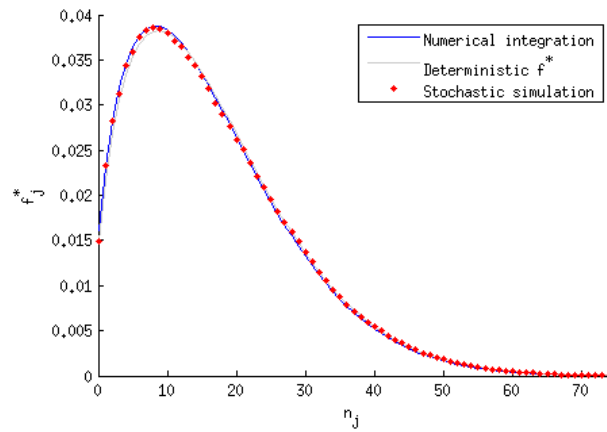


Figure B.1: Steady-state distribution of the number of patches in a given state calculated using three different methods, $K = 25$, $b = 1.05$ and $m = 0.1$. The stochastic simulation consisted of 500 patches.

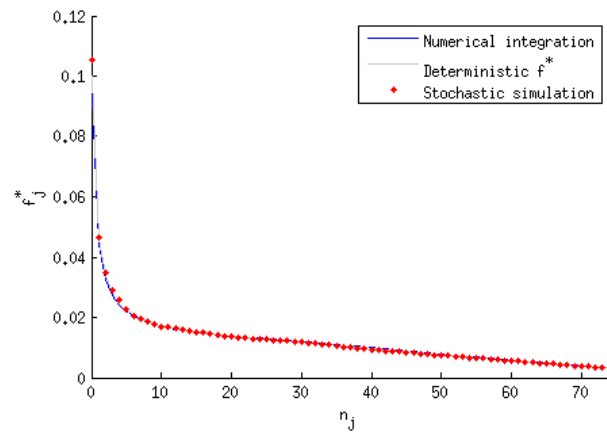


Figure B.2: Steady-state distribution of the number of patches in a given state calculated using three different methods, $b = 1.05$ and $m = 0.015$.